PNAS RESEARCH ARTICLE | CHEMISTRY

Syntheses of three-dimensional catenanes under kinetic control

Yong Wu[a], Qing-Hui Guo[b,c,1], Yunyan Qiu[a], Jacob A. Weber[a], Ryan M. Young[a], Laura Bancroft[a], Yang Jiao[a], Hongliang Chen[b,c], Bo Song[a], Wenqi Liu[a], Yuanning Feng (冯元宁)[a], Xingang Zhao[a], Xuesong Li[a], Long Zhang[a], Xiao-Yang Chen[a], Hao Li[b,c], Michael R. Wasielewski[a], and J. Fraser Stoddart[a,b,c,d,1]

Edited by Peter Stang, The University of Utah, Salt Lake City, UT; received October 9, 2021; accepted January 27, 2022

Although catenanes comprising two ring-shaped components can be made in large quantities by templation, the preparation of three-dimensional (3D) catenanes with cage-shaped components is still in its infancy. Here, we report the design and syntheses of two 3D catenanes by a sequence of S_N2 reactions in one pot. The resulting triply mechanically interlocked molecules were fully characterized in both the solution and solid states. Mechanistic studies have revealed that a suit[3]ane, which contains a three-fold symmetric cage component as the suit and a tribromide component as the body, is formed at elevated temperatures. This suit[3]ane was identified as the key reactive intermediate for the selective formation of the two 3D catenanes which do not represent thermodynamic minima. We foresee a future in which this particular synthetic strategy guides the rational design and production of mechanically interlocked molecules under kinetic control.

cationic cages | mechanically interlocked molecules | nontrivial topologies | suitanes | triple [π···π] interactions

Significance

During the past decades, the development of efficient methodologies for the creation of mechanically interlocked molecules (MIMs), such as catenanes and rotaxanes, has not only laid the foundation for the design and syntheses of artificial molecular machines (AMMs) but also opened up new research opportunities in multiple disciplines, ranging from contemporary chemistry to materials science. In this study, we describe a suitane-based strategy for the construction of three-dimensional (3D) catenanes, a subset of MIMs that are far from easy to make. Together with synthetic methodologies based on the metal coordination and dynamic covalent chemistry, this approach brings us one step closer to realizing routine syntheses of 3D catenanes.

While a number of catenanes consisting of multiple mechanically interlocked cyclic DNA (1, 2) and proteins (3, 4) have been found in living organisms, the creation of wholly synthetic analogs of these molecules—in an attempt to understand and harness their intrinsic physical, chemical, or biological properties—has inspired scientists for decades. The first chemical synthesis of a [2]catenane, which was reported in 1960 by Wasserman (5) using a statistical approach, was followed, in 1964, with the covalently directed templation of a [2]catenane involving more than 20 steps by Schill and Lüttringhaus (6). Since the early 1960s, the syntheses of catenanes progressed slowly, if hardly at all, during the subsequent 20 y. Over this period, catenane synthesis suffered from lengthy stepwise routes and/or low overall yields, resulting in only minuscule amounts of catenanes being produced and leaving their properties largely unexplored.

Using templation provided by metal ions to preorganize ligands into spatial arrangements that direct the formation of catenanes, Sauvage and coworkers (7) made a conceptual breakthrough in their synthesis in 1983. Since this time, much effort has been devoted to the development of new methodologies to effect the catenation of rings. These strategies have nearly always been accompanied (8, 9) by noncovalent bonding interactions, including, but not limited to, templation based on donor–acceptor (10), hydrogen-bonding (11, 12), and radical-pairing (13) interactions. The ever-expanding molecular-recognition toolbox, leading to efficient catenation, has enabled catenanes to become commonplace components in a variety of integrated systems, employing organic materials (14) and polymers (15) to fabricate molecular electronic devices (16) and create artificial molecular machines (17). Most of these catenanes, however, have been constructed from macrocyclic precursors, which are topologically two-dimensional (2D) in nature. The creation of catenanes composed of two or more three-dimensional (3D) cage-shaped components remains a challenge.

The formation of 3D catenanes (although all the catenanes are topologically 3D in nature, the term 3D catenanes used in this article refers specifically to catenanes consisting of multiple cage-shaped components) has relied on—with a few exceptions (18, 19)—self-assembly, in which the reversible formation of dynamic bonds acts as an error-checking mechanism to ensure the generation of thermodynamically favorable mechanically interlocked molecules (MIMs) in solution or during crystallization. The first example of the syntheses of 3D catenanes, which takes advantage of the dynamic metal–ligand coordinative bonds and hydrophobic interactions in water, was reported in 1999 by Fujita et al. (20). This approach has proved to be versatile for making metal-coordination-based 3D catenanes, as evidenced (21–36) by subsequent reports over the years. Besides metal–ligand interactions, several types of dynamic covalent

Author affiliations: [a]Department of Chemistry, Northwestern University, Evanston, IL 60208; [b]Stoddart Institute of Molecular Science, Department of Chemistry, Zhejiang University, Hangzhou 310027, China; [c]ZJU-Hangzhou Global Scientific and Technological Innovation Center, Hangzhou 311215, China; and [d]School of Chemistry, University of New South Wales, Sydney, NSW 2052, Australia

Author contributions: Y.W., Q.-H.G., and J.F.S. designed research; Y.W., J.A.W., R.M.Y., and L.B. performed research; B.S. and W.L. contributed new reagents/analytic tools; Y.W., Q.-H.G., Y.Q., Y.J., H.C., Y.F., X.Z., X.L., L.Z., X.-Y.C., H.L., M.R.W., and J.F.S. analyzed data; and Y.W., Q.-H.G., Y.Q., and J.F.S. wrote the paper.

The authors declare no competing interest.

This article is a PNAS Direct Submission.

[1]To whom correspondence may be addressed. Email: guoqhzju@zju.edu.cn or stoddart@northwestern.edu.

This article contains supporting information online at http://www.pnas.org/lookup/suppl/doi:10.1073/pnas.2118573119/-/DCSupplemental.

Published March 15, 2022.

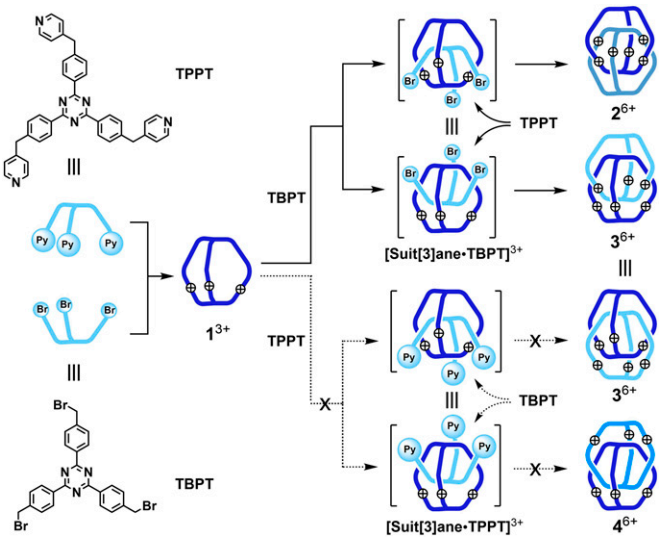

Fig. 1. Graphical representation of a suit[3]ane-based strategy for the selective syntheses of the two 3D catenanes $\mathbf{2}^{6+}$ and $\mathbf{3}^{6+}$. The reaction of **TPPT** with **TBPT** gives a tricationic monomeric cage $\mathbf{1}^{3+}$, which can open up its entrances at elevated temperatures and allow the slippage of **TBPT** into the cavity of $\mathbf{1}^{3+}$ to produce $[\mathbf{Suit[3]ane{\cdot}TBPT}]^{3+}$ as an intermediate. The subsequent reaction with **TPPT** from the bottom and top side of this intermediate affords the 3D catenanes $\mathbf{2}^{6+}$ and $\mathbf{3}^{6+}$, respectively. Since **TPPT** is relatively more bulky than **TBPT**, the formation of a similar $[\mathbf{Suit[3]ane{\cdot}TPPT}]^{3+}$ intermediate is disfavored kinetically as a result of steric hindrance. Thus, the 3D catenane $\mathbf{4}^{6+}$ cannot be formed.

chemistry, including the formation of imines (37, 38), boronic esters (39) and acylhydrazones (40), as well as alkyne metathesis (41), have been employed in the syntheses of 3D catenanes. Although these approaches are promising, the resulting catenanes oftentimes suffer from the use of precious metals in their syntheses and/or stability issues, limiting further applications. The development of new and efficient synthetic methodologies for the production of 3D catenanes remains a highly desirable pursuit.

Here, we present a facile strategy for the design and syntheses of a pair of 3D catenanes in one pot. The structures of both catenanes have been confirmed in both the solution and solid states. Moreover, mechanistic investigations reveal the importance of a suitane-based reaction pathway, in which a mechanically interlocked suit[3]ane with a trivial topology was identified as the reactive intermediate for the selective formation (Fig. 1) under kinetic control of the two 3D catenanes with nontrivial topologies.

Results

One-Pot Syntheses of 3D Catenanes. The syntheses of the monomeric cage $\mathbf{1}{\cdot}3CF_3CO_2$ and the 3D catenanes $\mathbf{2}{\cdot}6CF_3CO_2$ and $\mathbf{3}{\cdot}6CF_3CO_2$ (Fig. 2) started from two readily accessible precursors (*SI Appendix*, Figs. S1 and S2), namely 2,4,6-tris-[4-(4-pyridylmethyl)phenyl]-1,3,5-triazine (**TPPT**) and 2,4,6-tris-(4-bromomethylphenyl)-1,3,5-triazine (**TBPT**). Both **TPPT** and **TBPT** contain a triaryl triazine moiety, which tends to adopt a much flatter conformation compared with triaryl benzene (42) and favors [π···π] interactions (20). We began our investigation with the reaction between equimolar amounts of **TPPT** and **TBPT** at 50 °C for 3 d in *N*,*N*-dimethylformamide (DMF) in the presence of tetrabutylammonium iodide (TBAI) as a catalyst, followed by chromatographic purification, during which counterion exchange with trifluoroacetic acid (TFA) occurs to give the corresponding products. Although both starting materials were consumed, only trace amounts of 3D catenanes were obtained (*SI Appendix*, Table S1, Entry 1). When we changed the solvent to acetonitrile (MeCN), however,

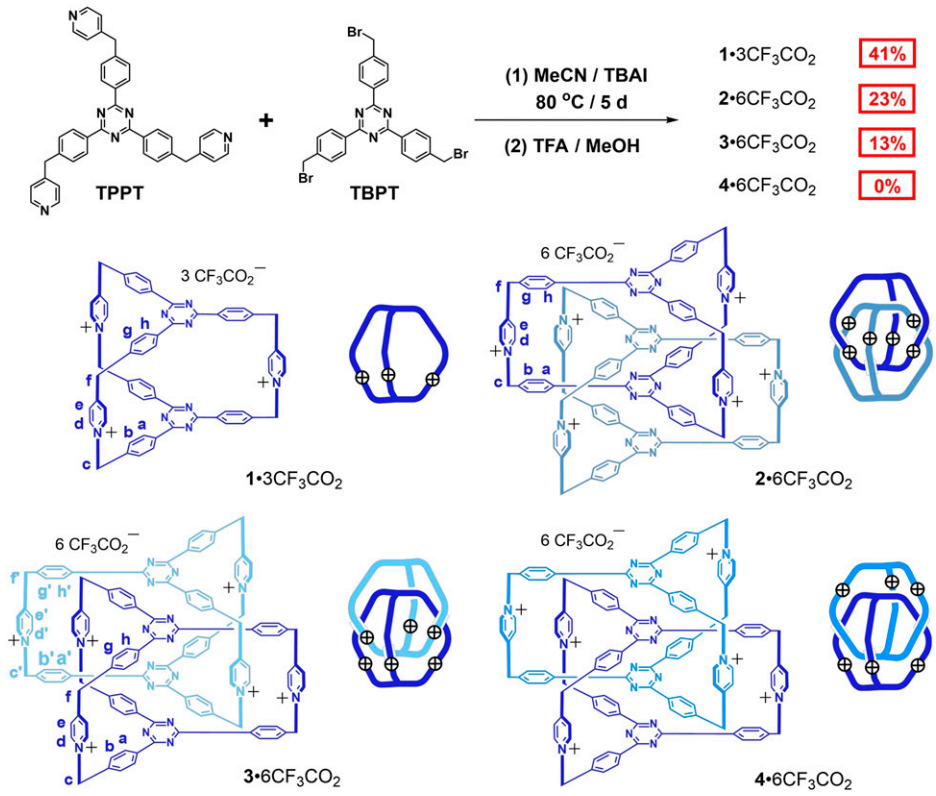

Fig. 2. One-pot syntheses of the monomeric cage $\mathbf{1}{\cdot}3CF_3CO_2$ and the 3D catenanes $\mathbf{2}{\cdot}6CF_3CO_2$ and $\mathbf{3}{\cdot}6CF_3CO_2$ from **TPPT** and **TBPT** using TBAI as a catalyst. The formation of another putative 3D catenane $\mathbf{4}{\cdot}6CF_3CO_2$ was, however, not observed.

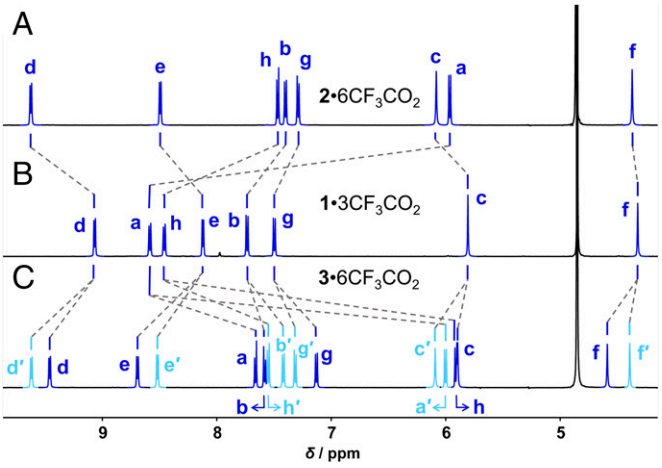

Fig. 3. Structural elucidation of $\mathbf{1}\cdot 3CF_3CO_2$, $\mathbf{2}\cdot 6CF_3CO_2$ and $\mathbf{3}\cdot 6CF_3CO_2$ by ^{1}H NMR (500 MHz, 298 K, CD_3OD) spectroscopy. ^{1}H NMR spectra of (*A*) $\mathbf{2}\cdot 6CF_3CO_2$, (*B*) $\mathbf{1}\cdot 3CF_3CO_2$, and (*C*) $\mathbf{3}\cdot 6CF_3CO_2$. The resonances corresponding to H_a (5.97 ppm) in $\mathbf{2}\cdot 6CF_3CO_2$, $H_{a'}$ (6.01 ppm) and H_h (5.91 ppm) in $\mathbf{3}\cdot 6CF_3CO_2$ show significant upfield shifts compared with those (8.58 ppm for H_a and 8.46 ppm for H_h) in $\mathbf{1}\cdot 3CF_3CO_2$. This observation is good evidence for the formation of MIMs, in which the inside protons are shielded by the other cage component.

the yields of the 3D catenanes $\mathbf{2}\cdot 6CF_3CO_2$ and $\mathbf{3}\cdot 6CF_3CO_2$ increased to 3% and 4%, respectively, most likely because MeCN sustains a larger solvophobic effect than DMF. This improvement in yields encouraged us to optimize this reaction by varying the solvent, temperature, reaction time and feeding ratio of the two reactants. The best result (*SI Appendix*, Table S1, Entry 7) was obtained after several rounds of optimization in which the monomeric cage $\mathbf{1}\cdot 3CF_3CO_2$ and the [2]catenanes $\mathbf{2}\cdot 6CF_3CO_2$ and $\mathbf{3}\cdot 6CF_3CO_2$ were isolated in 41%, 23%, and 13% yields, respectively. The formation of another putative 3D catenane $\mathbf{4}\cdot 6CF_3CO_2$, however, was not observed under a wide range of conditions.

Structural Characterization. The constitution of $\mathbf{1}\cdot 3CF_3CO_2$, and the co-constitutions of $\mathbf{2}\cdot 6CF_3CO_2$ and $\mathbf{3}\cdot 6CF_3CO_2$ were determined by ^{1}H nuclear magnetic resonance (NMR) spectroscopy. The ^{1}H NMR spectra of the 3D catenanes $\mathbf{2}\cdot 6CF_3CO_2$ (Fig. 3*A*) and $\mathbf{3}\cdot 6CF_3CO_2$ (Fig. 3*C*) differ significantly from that (Fig. 3*B*) of the monomeric cage $\mathbf{1}\cdot 3CF_3CO_2$. After making assignments to all the resonances in the ^{1}H NMR spectra of both 3D catenanes by employing a series of 2D NMR spectroscopic techniques (see *SI Appendix* for details), we found that the resonances in the ^{1}H NMR spectra, corresponding to H_a (5.97 ppm) in $\mathbf{2}\cdot 6CF_3CO_2$, and $H_{a'}$ (6.01 ppm) and H_h (5.91 ppm) in $\mathbf{3}\cdot 6CF_3CO_2$, undergo significant upfield shifts when compared with those (8.58 ppm for H_a, 8.46 ppm for H_h) arising in the ^{1}H NMR spectrum of $\mathbf{1}\cdot 3CF_3CO_2$. This observation is good evidence for the formation of MIMs, because once the triphenylenetriazine moiety is located within the cavity of the other cage component, the protons on the phenylene groups experience a strongly shielded magnetic environment. In contrast, the resonances corresponding to H_b, H_g, and H_h in $\mathbf{2}\cdot 6CF_3CO_2$ and $H_{b'}$, $H_{g'}$, $H_{h'}$, H_a, H_b, and H_g in $\mathbf{3}\cdot 6CF_3CO_2$ undergo relatively minor upfield shifts. This observation can be ascribed to the fact that these protons are located in less shielded magnetic fields. The resonances corresponding to all the protons on the pillars (H_c, H_d, H_e, and H_f in $\mathbf{2}\cdot 6CF_3CO_2$ and H_c, H_d, H_e, H_f, $H_{c'}$, $H_{d'}$, $H_{e'}$, and $H_{f'}$ in $\mathbf{3}\cdot 6CF_3CO_2$) undergo downfield shifts, an observation which can be explained by the fact that they are located in deshielded environments.

Both 3D catenanes $\mathbf{2}^{6+}$ and $\mathbf{3}^{6+}$ are achiral and belong to the point group, D_{3d} and C_{3v}, respectively. The catenane $\mathbf{3}^{6+}$ belongs to the same point group as its noninterlocked precursor $\mathbf{1}^{3+}$ for the simple reason that all six pyridinium units in $\mathbf{3}^{6+}$ point in the same direction, resulting in no changes in symmetry elements. In the case of $\mathbf{2}^{6+}$, however, the three pyridinium units in one cage component point in the opposite direction relative to those in the other cage, introducing three additional C_2 axes. As a consequence, this 3D catenane has a higher symmetry and belongs to the D_{3d} point group. Because σ symmetry elements are present in both co-constitutional isomers $\mathbf{2}^{6+}$ and $\mathbf{3}^{6+}$—in which the two mechanically interlocked components adopt staggered co-conformations—the dihedral angles in the different cage components are all 60° as a result of minimizing Coulombic repulsions between the six pyridinium units.

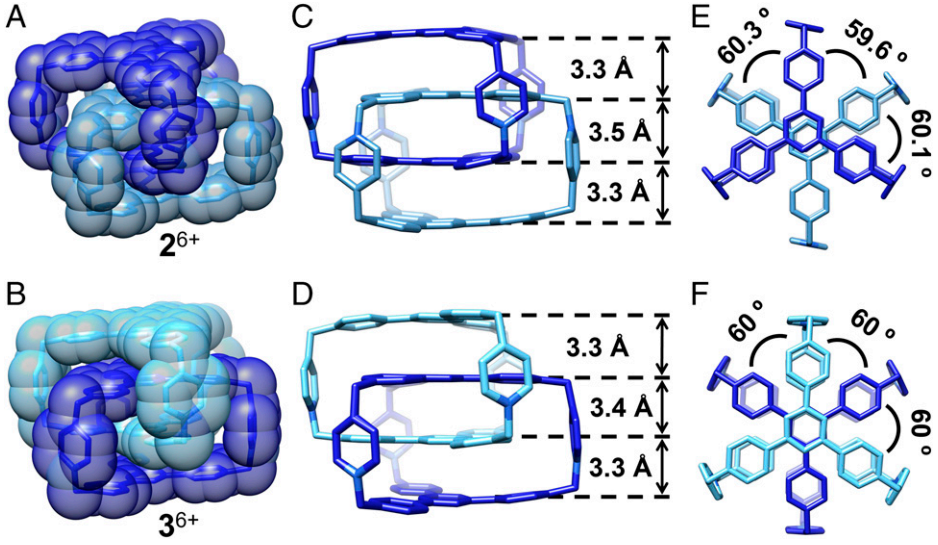

Fig. 4. X-ray single-crystal structures of the 3D catenanes $\mathbf{2}^{6+}$ and $\mathbf{3}^{6+}$. The two mechanically interlocked, identical cages are shown in royal blue and pale blue. Perspective views of (*A*) $\mathbf{2}^{6+}$ and (*B*) $\mathbf{3}^{6+}$ as stick representations with the corresponding semitransparent space-filling representations superimposed upon them. Side-on views of (*C*) $\mathbf{2}^{6+}$ and (*D*) $\mathbf{3}^{6+}$ as stick representations showing the plane-to-plane distances between two adjacent platforms. The distances are found to be 3.3 Å to 3.5 Å (i.e., ideal for [π···π] interactions). Plan views of (*E*) $\mathbf{2}^{6+}$ and (*F*) $\mathbf{3}^{6+}$ as stick representations showing the "dihedral angles". Irrelevant protons, $CF_3CO_2^-$ counterions and solvent molecules are omitted for the sake of clarity.

Single crystals (suitable for X-ray crystallography) of each of the 3D catenanes were obtained by slow vapor diffusion of iPr$_2$O into the corresponding MeOH solution at 252 and 298 K for **2**·6CF_3CO_2 and **3**·6CF_3CO_2, respectively. The solid-state structure of the monomeric cage $\mathbf{1}^{3+}$, which was also determined, showed a separation distance of 7.0 Å between the roof and the floor of the cage (*SI Appendix*, Fig. S3*C*). The single-crystal structures confirm (Fig. 4) unambiguously the formation of the two 3D catenanes, each consisting of two identical mechanically interlocked cage components. From the perspective views (Fig. 4 *A* and *B*), the efficient quadruple stacking of the aromatic platforms was observed for both $\mathbf{2}^{6+}$ and $\mathbf{3}^{6+}$. Side-on views (Fig. 4 *C* and *D*) revealed efficient [π···π] interactions between the two adjacent triphenylenetriazine platforms with plane-to-plane distances ranging from 3.3 to 3.5 Å in both $\mathbf{2}^{6+}$ and $\mathbf{3}^{6+}$. It is worthy of note that the separation distance (3.5 Å) between the inner triphenylenetriazine platforms of $\mathbf{2}^{6+}$ is slightly longer than that (3.4 Å) present in $\mathbf{3}^{6+}$, possibly because the repulsive interactions of positive charges in $\mathbf{2}^{6+}$ are stronger than those in $\mathbf{3}^{6+}$. From the plan view (Fig. 4*E*) of $\mathbf{2}^{6+}$, it is found that the triazine cores of the two cage components are displaced slightly with respect to each other. This perturbation is, however, not present in the structure (Fig. 4*F*) of $\mathbf{3}^{6+}$. We speculate that the differences in relative geometries of the cage components might result from the crystal packing preference at different temperatures. When crystals of $\mathbf{2}^{6+}$ were grown at low temperature (252 K), the crystals obtained were those with increased noncovalent bonding interactions between the two mechanically interlocked components. This interpretation is consistent with the fact that [CH···π] interactions, in addition to [π···π] interactions, are present in $\mathbf{2}^{6+}$ as revealed (43, 44) by an independent gradient model (IGM) analysis (*SI Appendix*, Fig. S6).

Mechanism. Mechanistic investigations into the synthetic strategy, not only provided insight into the formation of **2**·6CF_3CO_2 and **3**·6CF_3CO_2, but more importantly also shed light on what we believe to be new design principles for the syntheses of 3D catenanes in general. Theoretically, three different catenanes (*SI Appendix*, Fig. S14) can be formed by the reaction of **TPPT** with **TBPT**, including $\mathbf{2}^{6+}$, $\mathbf{3}^{6+}$, and another C_3-symmetric 3D catenane $\mathbf{4}^{6+}$ with all the positive charges pointing outward. The theoretical formation probabilities of $\mathbf{2}^{6+}$, $\mathbf{3}^{6+}$, and $\mathbf{4}^{6+}$ were calculated (*SI Appendix*, Fig. S14) to be 25%, 50%, and 25%, respectively. Density functional theory (DFT) calculations reveal (*SI Appendix*, Fig. S15) that the relative energies of $\mathbf{2}^{6+}$, $\mathbf{3}^{6+}$, and $\mathbf{4}^{6+}$ are 20.8, 11.5, and 0 kcal/mol, respectively. Although $\mathbf{4}^{6+}$ has the lowest relative energy, no product corresponding to this 3D catenane was observed under all the conditions explored (*SI Appendix*, Table S1)—suggesting that the formation of the 3D catenanes $\mathbf{2}^{6+}$ and $\mathbf{3}^{6+}$ is not taking place under thermodynamic control, which has been proposed for the formation of other 3D catenanes reported in the literature for approaches involving both metal coordination (20–36) and dynamic covalent chemistry (37–41).

Given the fact that the monomeric cage $\mathbf{1}^{3+}$ was isolated in a good yield—41% under the optimized conditions—and the plane-to-plane separation distance in the solid-state structure of $\mathbf{1}^{3+}$ is 7.0 Å— *SI Appendix*, Fig. S3*C*—we propose a suitane-based mechanism based on the near-perfect cofacial [π···π] stacking interactions between the suit $\mathbf{1}^{3+}$ and an aromatic torso (*SI Appendix*, Fig. S16). We assume that the first step in the formation of the 3D catenanes $\mathbf{2}^{6+}$ and $\mathbf{3}^{6+}$ is the generation of a monomeric cage $\mathbf{1}^{3+}$, which opens up its entrances at elevated temperatures and allows the slippage of **TBPT** into the cavity of $\mathbf{1}^{3+}$ to produce [**Suit[3]ane·TBPT**]$^{3+}$ as an intermediate. The subsequent reaction with **TPPT** from the bottom and top side of this intermediate affords the 3D catenanes $\mathbf{2}^{6+}$ and $\mathbf{3}^{6+}$, respectively (reaction pathway A in *SI Appendix*, Fig. S16). Because **TPPT** is relatively more bulky than **TBPT**, the formation of a similar [**Suit[3]ane·TPPT**]$^{3+}$ intermediate is disfavored kinetically as a result of steric hindrance. Thus, neither $\mathbf{3}^{6+}$ nor $\mathbf{4}^{6+}$ can be formed by the reaction pathway B (*SI Appendix*, Fig. S16).

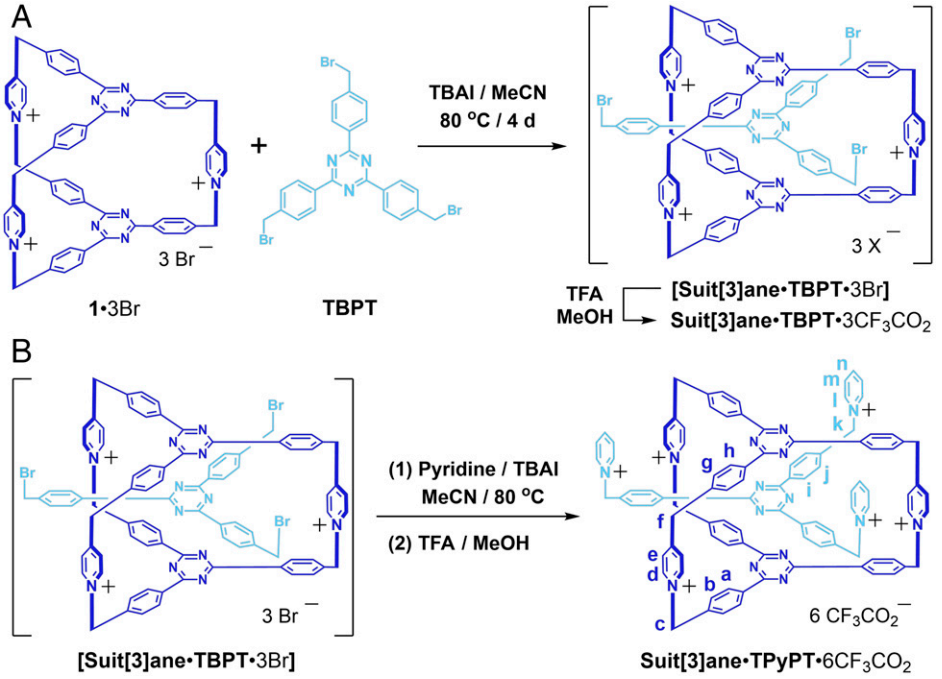

Fig. 5. Mechanistic study. (*A*) Generation of the reactive intermediate [**Suit[3]ane·TBPT**·3Br] and subsequent counterion exchange to give **Suit[3]ane·TBPT**·3CF_3CO_2. This compound, however, can be easily hydolyzed at room temperature so only mass spectrum was recorded. (*B*) Capturing of the reactive intermediate [**Suit[3]ane·TBPT**·3Br] by reacting it with pyridine in the presence of TBAI to form **Suit[3]ane·TPyPT**·6CF_3CO_2, which is stable during column purification using H_2O and MeCN as the eluent and can be fully characterized.

In order to verify the proposed hypothesis, a mixture of **1**·3Br and **TBPT** was stirred (Fig. 5*A*) at 80 °C for 4 d in MeCN in the presence of TBAI. The crude reaction mixture was analyzed by ^{1}H NMR spectroscopy (*SI Appendix*, Fig. S18*A*) and two doublets were identified at 9.50 (J = 7.0 Hz) and 6.36 ppm (J = 8.2 Hz). This observation suggests that a [**Suit[3]ane·TBPT**·3Br] intermediate with **TBPT** trapped inside the cavity of **1**·3Br has been formed. Whereas, in a control experiment using **TPPT** instead of **TBPT** to perform the same reaction (*SI Appendix*, Fig. S17), neither downfield nor upfield-shifted doublets can be detected in the ^{1}H NMR spectrum (*SI Appendix*, Fig. S18*B*), indicating that **TPPT** is not able to slip into the cavity of **1**·3Br to form the [**Suit[3]ane·TPPT**·3Br] intermediate under the same reaction conditions.

In an attempt to obtain convincing evidence for the proposed mechanism, we tried to isolate and characterize the reaction intermediate [**Suit[3]ane·TBPT**]$^{3+}$. After counterion exchange with TFA (Fig. 5*A*), the crude mixture containing **Suit[3]ane·TBPT**·3CF_3CO_2 was purified by reversed-phase column chromatography and analyzed by high resolution electrospray ionization mass spectrometry (ESI-MS). The mass spectrum (Fig. 6*A*) of **Suit[3]ane·TBPT**·3CF_3CO_2 exhibited prominent peaks at m/z = 505.1028 (calculated for [**Suit[3]ane·TBPT**]$^{3+}$ m/z = 505.1022) and 814.1469 (calculated for [**Suit[3]ane·TBPT**·CF_3CO_2]$^{2+}$ m/z = 814.1462), confirming the formation of the proposed suit[3]ane intermediate.

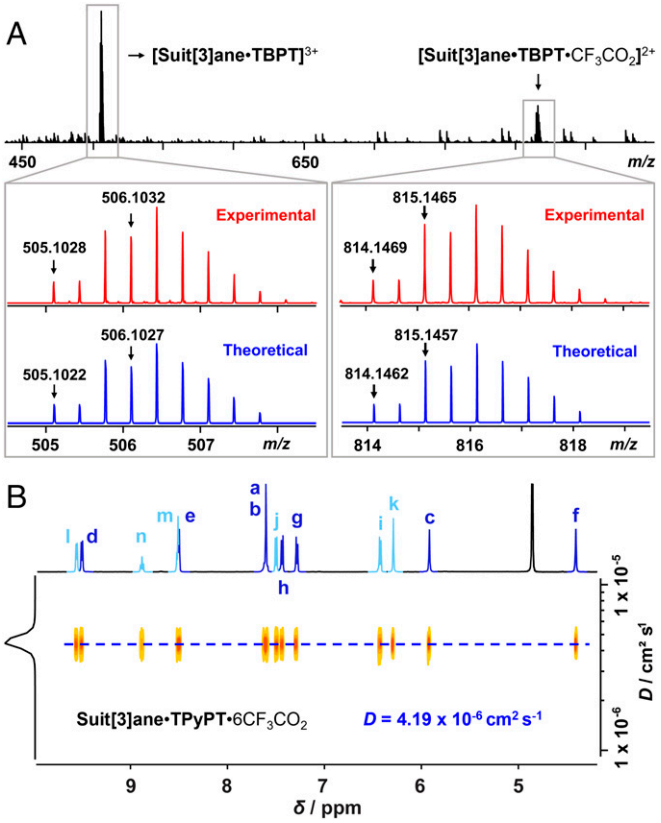

Fig. 6. Characterization of the suit[3]ane intermediate. (*A*) Mass spectrum of **Suit[3]ane·TBPT**·3CF_3CO_2. The labeled m/z signals correspond to those of species that lose different numbers (3, 2) of $CF_3CO_2^-$ counterions. The corresponding theoretical peaks (blue) of [**Suit[3]ane·TBPT**]$^{3+}$ and [**Suit[3]ane•TBPT**·CF_3CO_2]$^{2+}$, shown in the expanded spectra, were found to be consistent with the experimental peaks (red). (*B*) ^{1}H DOSY NMR spectrum (600 MHz, 298 K, CD_3OD) of **Suit[3]ane·TPyPT**·6CF_3CO_2 revealed a single diffusion coeffiecient (D = 4.19 × 10^{-6} cm^2 s^{-1}) for all of its proton resonances. This observation confirms that all these resonances belong to a single molecule.

Characterization of **Suit[3]ane·TBPT**·3CF_3CO_2 by NMR spectroscopy was, however, not successful because this compound was found to hydrolyze over time at room temperature. Further evidence of the water-labile nature of **Suit[3]ane·TBPT**·3CF_3CO_2 was provided by ESI-MS analysis (*SI Appendix*, Fig. S19).

In order to overcome the problem of isolating and characterizing the reactive intermediate, we reacted (Fig. 5*B*) it with pyridine to obtain a stable compound (i.e., **Suit[3]ane·TPyPT**·6CF_3CO_2), which was isolated and fully characterized. The diffusion-ordered spectroscopy (DOSY) NMR spectrum (Fig. 6*B*) of **Suit[3]ane·TPyPT**·6CF_3CO_2 revealed a single diffusion coefficient (D = 4.19 × 10^{-6} cm^2 s^{-1}) for all of its proton resonances. This observation confirms that all these resonances belong to a single molecule. The structure of **Suit[3]ane·TPyPT**·6CF_3CO_2 was also confirmed by mass spectrometry (*SI Appendix*, Fig. S21). All these computational results and experimental evidence support the proposed suit[3]ane-based mechanism for the selective formation of the 3D catenanes $\mathbf{2}^{6+}$ and $\mathbf{3}^{6+}$.

Conclusions

We have shown that two 3D catenanes, namely $\mathbf{2}^{6+}$ and $\mathbf{3}^{6+}$ with nontrivial topologies, can be synthesized in 23% and 13% yields, respectively, by a sequence of facile S_N2 reactions in one pot. Each of these two 3D catenanes is composed of two mechanically interlocked triangular prisms and comprises six pyridinium pillars. On account of the Coulombic repulsions between these pyridinium units, neither $\mathbf{2}^{6+}$ nor $\mathbf{3}^{6+}$ represents the most thermodynamically favored product. It is noteworthy that another putative isomeric catenane, namely $\mathbf{4}^{6+}$, which is able to locate its six positively charged pyridinium nitrogen atoms in a relatively remote manner, is more thermodynamically stable than either $\mathbf{2}^{6+}$ or $\mathbf{3}^{6+}$. Mechanistic studies, however, revealed that a suit[3]ane—containing a triangular component with three benzylbromide units (**TBPT**) that becomes mechanically interlocked within the cavity of a C_3-symmetric cage-shaped component—represents the key reactive intermediate for the selective formation of the 3D catenanes $\mathbf{2}^{6+}$ and $\mathbf{3}^{6+}$. In contrast, the formation of the putative suit[3]ane containing **TPPT** is disfavored kinetically because of the large steric hindrance preventing its formation. The fact that the suit[3]ane containing **TPPT** is not formed during the reaction means that the 3D catenane $\mathbf{4}^{6+}$ cannot be obtained under kinetic control. Considering the well-developed methodologies (45–50) for the construction of suitanes, this suit[3]ane-based strategy opens up what we believe to be new opportunities for synthesizing 3D catenanes and other topologically nontrivial molecules (51–54) which do not correspond to thermodynamic minima. Such coconformations are unlikely to be obtained by previously reported methods (20–41) that rely on dynamic bond formation.

Materials and Methods

All reagents were purchased from commercial suppliers (MilliporeSigma or Fisher) and used without further purification. **TPPT** and **TBPT** were synthesized according to protocols described previously (20, 55) with slight modifications (56).

Syntheses of 1•3CF_3CO_2/2•6CF_3CO_2/3•6CF_3CO_2. A catalytic amount of TBAI (2.5 mg, 6.9 μmol, 0.2 eq.) was added to a suspension of **TPPT** (20.0 mg, 34.3 μmol, 1.0 eq.) and **TBPT** (25.0 mg, 42.9 μmol, 1.25 eq.) in anhydrous MeCN (40 mL) under a N_2 atmosphere. The reaction mixture was heated at 80 °C and stirred for 5 d. After evaporation to remove all the solvent, TFA (2 mL) and MeOH (10 mL) were added to the residue and the resulting mixture was stirred for an additional 30 min. The concentrated residue was loaded onto a

CombiFlash chromatography system and purified on a C_{18} reversed-phase column using a mixture of 0.1% vol/vol TFA in H_2O and 0.1% vol/vol TFA in MeCN. Fractions containing the product were combined and concentrated. The crude product was then subjected to purification on a preparative reversed-phase HPLC system with H_2O/MeCN (67/33, vol/vol, both containing 0.1% vol/vol TFA) as the eluent, affording **1**·3CF_3CO_2 (17.9 mg, 41% yield), **2**·6CF_3CO_2 (10.0 mg, 23% yield) and **3**·6CF_3CO_2 (5.7 mg, 13% yield) as white solids.

Data Availability. All study data are included in the article and/or *SI Appendix*. All single-crystal data have been deposited to the Cambridge Crystallographic Data Centre (CCDC) and can be downloaded free of charge from https://www.ccdc.cam.ac.uk/structures/. The reference numbers of **1**·3PF_6, **2**·6CF_3CO_2, and **3**·6CF_3CO_2 are CCDC 2114507, 2114508, and 2114509, respectively.

ACKNOWLEDGMENTS. Financial support from Northwestern University (NU) is gratefully acknowledged. This work was supported by the National Science Foundation (DMR-2003739 to M.R.W.) and the Starry Night Science Fund of Zhejiang University Shanghai Institute for Advanced Study (SN-ZJU-SIAS-006 to H.L., Q.-H.G., and H.C.). Q.-H.G. and H.C. thank ZJU-Hangzhou Global Scientific and Technological Innovation Center for generous startup funding. Q.-H.G. thanks the National Natural Science Foundation of China (22193020 and 22193022). This work made use of the IMSERC at NU, which receives support from the National Institutes of Health (1S10OD012016-01/1S10RR019071-01A1), Soft and Hybrid Nanotechnology Experimental Resource (NSF ECCS-1542205), the state of Illinois, and the International Institute for Nanotechnology. We thank Dr. Yang Yu at NU for assistance in HPLC experiments.

1. B. Hudson, J. Vinograd, Catenated circular DNA molecules in HeLa cell mitochondria. *Nature* **216**, 647–652 (1967).
2. D. A. Clayton, J. Vinograd, Circular dimer and catenate forms of mitochondrial DNA in human leukaemic leucocytes. *Nature* **216**, 652–657 (1967).
3. W. R. Wikoff *et al.*, Topologically linked protein rings in the bacteriophage HK97 capsid. *Science* **289**, 2129–2133 (2000).
4. D. R. Boutz, D. Cascio, J. Whitelegge, L. J. Perry, T. O. Yeates, Discovery of a thermophilic protein complex stabilized by topologically interlinked chains. *J. Mol. Biol.* **368**, 1332–1344 (2007).
5. E. Wasserman, The preparation of interlocking rings: A catenane. *J. Am. Chem. Soc.* **82**, 4433–4434 (1960).
6. G. Schill, A. Lüttringhaus, The preparation of catena compounds by directed synthesis. *Angew. Chem. Int. Ed. Engl.* **3**, 546–547 (1964).
7. C. O. Dietrich-Buchecker, J.-P. Sauvage, J.-P. Kintzinger, Une nouvelle famille de molecules: Les metallo-catenanes. *Tetrahedron Lett.* **24**, 5095–5098 (1983).
8. J.-P. Sauvage, C. O. Dietrich-Buchecker, Eds., *Molecular Catenanes, Rotaxanes and Knots* (John Wiley & Sons, Ltd, 1999).
9. G. Gil-Ramírez, D. A. Leigh, A. J. Stephens, Catenanes: Fifty years of molecular links. *Angew. Chem. Int. Ed.* **54**, 6110–6150 (2015).
10. P. R. Ashton *et al.*, A [2]catenane made to order. *Angew. Chem. Int. Ed. Engl.* **28**, 1396–1399 (1989).
11. C. A. Hunter, Synthesis and structure elucidation of a new [2]-catenane. *J. Am. Chem. Soc.* **114**, 5303–5311 (1992).
12. M. R. Sambrook, P. D. Beer, J. A. Wisner, R. L. Paul, A. R. Cowley, Anion-templated assembly of a [2]catenane. *J. Am. Chem. Soc.* **126**, 15364–15365 (2004).
13. J. C. Barnes *et al.*, A radically configurable six-state compound. *Science* **339**, 429–433 (2013).
14. S. Mena-Hernando, E. M. Pérez, Mechanically interlocked materials. Rotaxanes and catenanes beyond the small molecule. *Chem. Soc. Rev.* **48**, 5016–5032 (2019).
15. L. F. Hart *et al.*, Material properties and applications of mechanically interlocked polymers. *Nat. Rev. Mater.* **6**, 508–530 (2021).
16. H. Chen, J. F. Stoddart, From molecular to supramolecular electronics. *Nat. Rev. Mater.* **6**, 804–828 (2021).
17. C. J. Bruns, J. F. Stoddart, *The Nature of the Mechanical Bond* (John Wiley & Sons, Ltd, 2016).
18. Y. Li *et al.*, Sulfate anion templated synthesis of a triply interlocked capsule. *Chem. Commun.* **46**, 7134–7136 (2009).
19. D. Chakraborty, R. Modak, P. Howlader, P. S. Mukherjee, *De novo* approach for the synthesis of water-soluble interlocked and non-interlocked organic cages. *Chem. Commun.* **57**, 3995–3998 (2021).
20. M. Fujita, N. Fujita, K. Ogura, K. Yamaguchi, Spontaneous assembly of ten components into two interlocked, identical coordination cages. *Nature* **400**, 52–55 (1999).
21. Y. Yamauchi, M. Yoshizawa, M. Fujita, Engineering stacks of aromatic rings by the interpenetration of self-assembled coordination cages. *J. Am. Chem. Soc.* **130**, 5832–5833 (2008).
22. M. Fukuda, R. Sekiya, R. Kuroda, A quadruply stranded metallohelicate and its spontaneous dimerization into an interlocked metallohelicate. *Angew. Chem. Int. Ed.* **47**, 706–710 (2008).
23. A. Westcott, J. Fisher, L. P. Harding, P. Rizkallah, M. J. Hardie, Self-assembly of a 3-D triply interlocked chiral [2]catenane. *J. Am. Chem. Soc.* **130**, 2950–2951 (2008).
24. X. Kuang *et al.*, Assembly of a metal-organic framework by sextuple intercatenation of discrete adamantane-like cages. *Nat. Chem.* **2**, 461–465 (2010).
25. J. Heine, J. Schmedt auf der Günne, S. Dehnen, Formation of a strandlike polycatenane of icosahedral cages for reversible one-dimensional encapsulation of guests. *J. Am. Chem. Soc.* **133**, 10018–10021 (2011).
26. S. Freye *et al.*, Allosteric binding of halide anions by a new dimeric interpenetrated coordination cage. *Angew. Chem. Int. Ed.* **51**, 2191–2194 (2012).
27. A. Mishra *et al.*, Molecular self-assembly of arene-Ru based interlocked catenane metalla-cages. *Chem. Commun.* **50**, 7542–7544 (2014).
28. D. Samanta, P. S. Mukherjee, Sunlight-induced covalent marriage of two triply interlocked Pd_6 cages and their facile thermal separation. *J. Am. Chem. Soc.* **136**, 17006–17009 (2014).
29. L. Yang *et al.*, Binding of anions in triply interlocked coordination catenanes and dynamic allostery for dehalogenation reactions. *Chem. Sci.* **9**, 1050–1057 (2017).
30. W.-Z. Qiao, T.-Q. Song, P. Cheng, B. Zhao, Highly selective enamination of β-ketoesters catalyzed by interlocked [Cu_8] and [Cu_{18}] nanocages. *Angew. Chem. Int. Ed.* **58**, 13302–13307 (2019).
31. Y. Wang *et al.*, A cyclic bis[2]catenane metallacage. *Nat. Commun.* **11**, 2727 (2020).
32. T. K. Ronson, Y. Wang, K. Baldridge, J. S. Siegel, J. R. Nitschke, An S_{10}-symmetric 5-fold interlocked [2]catenane. *J. Am. Chem. Soc.* **142**, 10267–10272 (2020).
33. Y.-W. Zhang, S. Bai, Y.-Y. Wang, Y.-F. Han, A strategy for the construction of triply interlocked organometallic cages by rational design of poly-NHC precursors. *J. Am. Chem. Soc.* **142**, 13614–13621 (2020).
34. L. Cheng *et al.*, Three-dimensional polycatenation of a uranium-based metal–organic cage: Structural complexity and radiation detection. *J. Am. Chem. Soc.* **142**, 16218–16222 (2020).
35. Y.-Y. Zhang, F.-Y. Qiu, H.-T. Shi, W. Yu, Self-assembly and guest-induced disassembly of triply interlocked [2]catenanes. *Chem. Commun.* **57**, 3010–3013 (2021).
36. L.-X. Cai *et al.*, Controlled self-assembly and multistimuli-responsive interconversions of three conjoined twin-cages. *J. Am. Chem. Soc.* **143**, 2016–2024 (2021).
37. T. Hasell *et al.*, Triply interlocked covalent organic cages. *Nat. Chem.* **2**, 750–755 (2010).
38. P. Li *et al.*, De novo construction of catenanes with dissymmetric cages by space-discriminative post-assembly modification. *Angew. Chem. Int. Ed.* **59**, 7113–7121 (2020).
39. G. Zhang, O. Presly, F. White, I. M. Oppel, M. Mastalerz, A shape-persistent quadruply interlocked giant cage catenane with two distinct pores in the solid state. *Angew. Chem. Int. Ed.* **53**, 5126–5130 (2014).
40. H. Li *et al.*, Quantitative self-assembly of a purely organic three-dimensional catenane in water. *Nat. Chem.* **7**, 1003–1008 (2015).
41. Q. Wang *et al.*, Solution-phase dynamic assembly of permanently interlocked aryleneethynylene cages through alkyne metathesis. *Angew. Chem. Int. Ed.* **54**, 7550–7554 (2015).
42. T. Jiao, G. Wu, L. Chen, C.-Y. Wang, H. Li, Precursor control over the self-assembly of organic cages *via* imine condensation. *J. Org. Chem.* **83**, 12404–12410 (2018).
43. C. Lefebvre *et al.*, Accurately extracting the signature of intermolecular interactions present in the NCI plot of the reduced density gradient versus electron density. *Phys. Chem. Chem. Phys.* **19**, 17928–17936 (2017).
44. T. Lu, F. Chen, Multiwfn: A multifunctional wavefunction analyzer. *J. Comput. Chem.* **33**, 580–592 (2012).
45. A. R. Williams *et al.*, Suitanes. *Angew. Chem. Int. Ed.* **45**, 6665–6669 (2006).
46. B. H. Northrop, F. Aricó, N. Tangchiavang, J. D. Badjić, J. F. Stoddart, Template-directed synthesis of mechanically interlocked molecular bundles using dynamic covalent chemistry. *Org. Lett.* **8**, 3899–3902 (2006).
47. A. Pun, D. A. Hanifi, G. Kiel, E. O'Brien, Y. Liu, Facile route to an all-organic, triply threaded, interlocked structure by templated dynamic clipping. *Angew. Chem. Int. Ed.* **51**, 13119–13122 (2012).
48. K. Zhu, G. Baggi, V. N. Vukotic, S. J. Loeb, Reversible mechanical protection: Building a 3D "suit" around a T-shaped benzimidazole axle. *Chem. Sci.* **8**, 3898–3904 (2017).
49. W. Liu, C. L. Stern, J. F. Stoddart, Suit[4]ane. *J. Am. Chem. Soc.* **142**, 10273–10278 (2020).
50. X.-Y. Chen *et al.*, Suit[3]ane. *J. Am. Chem. Soc.* **142**, 20152–20160 (2020).
51. K. S. Chichak *et al.*, Molecular Borromean rings. *Science* **304**, 1308–1312 (2004).
52. T. Sawada, Y. Inomata, K. Shimokawa, M. Fujita, A metal-peptide capsule by multiple ring threading. *Nat. Commun.* **10**, 5687 (2019).
53. J. F. Stoddart, Dawning of the age of molecular nanotopology. *Nano Lett.* **20**, 5597–5600 (2020).
54. Q.-H. Guo, Y. Jiao, Y. Feng, J. F. Stoddart, The rise and promise of molecular nanotopology. *CCS Chem.* **3**, 1542–1572 (2021).
55. J. Fan, J. W. Bats, M. Schmittel, Combining dynamic heteroleptic complex formation with constitutional dynamic synthesis: A facile way to M3LL' cage assemblies. *Inorg. Chem.* **48**, 6338–6340 (2009).
56. S. Duez, A. K. Steib, S. M. Manolikakes, P. Knochel, Lewis acid promoted benzylic cross-couplings of pyridines with aryl bromides. *Angew. Chem. Int. Ed.* **50**, 7686–7690 (2011).